EXAFS analysis of the structural evolution of gel-formed La_2O_3

Fatima Ali,[a,b] Alan V. Chadwick[a] and Mark E. Smith*[b]

[a]*Department of Chemistry, University of Kent, Canterbury, Kent, UK CT2 7NH*
[b]*Department of Physics, University of Kent, Canterbury, Kent, UK CT2 7NR*

Sol–gel-produced La_2O_3, derived from the hydrolysis and subsequent calcination of lanthanum isopropoxide, has been investigated by EXAFS of the La L_{III} edge. The evolution of the local structure through a series of amorphous intermediate states has been modelled by three shells, two lanthanum–oxygen and the other lanthanum–lanthanum. For comparison, well characterised bulk $La(OH)_3$, LaO(OH) and La_2O_3 were examined using EXAFS. The sol–gel-prepared oxide was more disordered and had significantly smaller particles than the oxide prepared by calcination of $La_2(CO_3)_3$ after the same heat treatments. For the gels in the intermediate states, well defined La–O shells are seen but the La–La shells are characterised by large Debye–Waller factors. Comparison of these results with previous ^{17}O solid-state NMR on a similar set of samples has some significant implications for the sensitivity to disorder of these important atomic-scale probes.

Sol–gel production of materials offers a route for the formation of nanocrystalline powders. Nanocrystalline materials can exhibit greatly modified properties compared to bulk polycrystalline solids, such as increased plastic deformation at relatively low temperatures, as observed in TiO_2.[1] Heat treatment causes sintering and growth of powder particles which involve structural changes. Probing the atomic-scale structure of such materials allows a better understanding of the consolidation process and opens up the possibility of systematically tailoring the powder properties (*e.g.* crystallinity, particle size, phase content). The largely amorphous nature of these samples means that atomic-scale characterisation probes must be applied.

Extended X-ray absorption fine structure (EXAFS) spectroscopy is a local structural probe which enables the structure around a specific probe atom to be determined accurately.[2,3] EXAFS is the oscillations in the X-ray absorption coefficient that occur above the absorption edge required for the emission of a photoelectron from a core (K or L) shell. The oscillations arise from the interference of the outgoing photoelectron with that part of itself that is backscattered by atoms surrounding the excited atom. The oscillations contain information on the nature of the backscattering atoms, their number and distance from the target atom. EXAFS, unlike Bragg diffraction, does not rely on long-range order and can be used to study local structure in liquids, as well as amorphous and crystalline solids.

Characterising the lanthanum environment in La_2O_3 powders prepared by various methods, particularly from calcination of $La_2(CO_3)_3$ and from hydrolysis of lanthanum isopropoxide, would be of much interest given the wide technological applications of La_2O_3. It acts as a supported catalyst for the oxidative coupling of methane and for hydrogenation.[4] In many of its applications it is often doped, so that the kinetics details of the oxide production of the different components involved are of key importance, particularly to guard against segregation and non-uniform doping. For example, La_2O_3 doped with SrO is an important catalyst for methane coupling[5] and it is also a good ion conductor at elevated temperatures.[6]

Previously, solid-state ^{17}O NMR has been reported from La_2O_3, LaO(OH), $La(OH)_3$ and an La_2O_3 gel.[7] It was an intriguing observation that, unlike sol–gel production of other oxides such as TiO_2 and ZrO_2, the gel first formed LaO(OH) prior to conversion to La_2O_3. For LaO(OH) the NMR linewidth was characteristic of local order, despite only a broad ill-defined X-ray pattern being observed, indicating that the sample was nanocrystalline. Lanthanum EXAFS of the L_{III} edge is complicated by the close proximity of the L_{II} edge that truncates the useful range over which data can be collected. Simulation of the EXAFS data is also complicated by the complex lanthanum coordination polyhedra with La–O and La–La distances varying quite considerably. Some simplified models have to be introduced to reduce the number of parameters to a number that can be reasonably fitted, given the experimental data. Such analysis has been used in other studies for the La L_{III} edge using a three-shell model, which well approximated the complex structures.[8] Such an approach is also adopted here. A relatively limited number of previous lanthanum EXAFS studies have been reported, including the nature of the defect sites in Sr-doped La_2O_3.[9] For fluorozirconate glasses the lanthanum environment was found to be very similar to that in crystalline LaF_3.[10] In K_2O–La_2O_3–SiO_2 glasses the electron density around the lanthanum atom appeared to increase with lanthanum content, while the average symmetry of its local environment decreased, while from the EXAFS measurements in these glasses the average La–O distance and coordination number remained quite constant with composition.[11] Glasses from the La–Ga–S system have also been studied and it was shown that the lanthanum coordination in the crystalline and glassy state was the same.[12] EXAFS of La_2CuO_4 showed the lanthanum to be nine-fold coordinated by oxygen.[13]

Experimental

La_2O_3 can be produced by direct thermal decomposition of the carbonate at 900 °C. To form $La(OH)_3$, La_2O_3 was sealed in a Pyrex ampoule with a slight excess of H_2O over that required for complete conversion to $La(OH)_3$. The ampoule was heated at 110 °C for 72 h and then dried under a vacuum at room temperature. The $La(OH)_3$ was then heated in an alumina boat under a stream of dry nitrogen for 90 min at 325 °C, producing LaO(OH). Some of this sample was heated at 700 °C for 30 min. The sol–gel preparation used 99.9% lanthanum isopropoxide (Johnson Matthey), $La(OC_3H_7)_3$, which was initially cooled to dry-ice temperature (−80 °C). A mixture of water and ethanol (1 : 4 molar ratio) was dropped onto the lanthanum isopropoxide until just enough water had been added for complete hydrolysis. The resulting cloudy solution was allowed to warm to room temperature over 2 h in a dry glovebox, with continuous stirring. The gel that formed had any excess water and solvent removed by evacu-

ation at room temperature and the resulting powder was successively heated to 100, 200, 350, 500, 700 and 1000 °C for 2 h periods. After each heating the sample was quenched to room temperature, with some removed for XRD and EXAFS analysis and the rest recrushed. An *in situ* EXAFS experiment was carried out where the initial gel preparation was as above, before transferring to the sample holder, where it was heated to the successive temperatures and held at each for about 1 h.

X-Ray powder diffraction patterns for all samples were collected on a Phillips PW1050 powder diffractometer using Cu-Kα radiation ($\lambda = 0.1544$ nm). A range of $2\theta = 20$–$100°$ was scanned at a rate of $1° \text{ min}^{-1}$. An estimate of the particle size (S) was made by applying the Scherrer equation, *i.e.* $S = K\lambda/\beta \cos\theta$, where K is a constant (0.89), β is the full width at half maximum of a diffraction peak at angle θ and λ is the X-ray wavelength.

EXAFS measurements on the La L_{III} absorption edge were performed on station 7.1 at the CCLRC Daresbury Synchrotron Radiation Source. The synchrotron has an electron energy of 2 GeV and the average beam current during the measurements was 200 mA. An order-sorting, double silicon(111) crystal monchromator was employed and the harmonic rejection was set at 50%. The spectra were collected in transmission mode. The samples were prepared by grinding the materials in an agate pestle and mortar, mixing thoroughly with fine silica powder and formed into pellets in a 13 mm IR press. The thicknesses of the pellets were adjusted to give an absorption edge jump (ln[incident beam intensity]/[transmitted beam intensity]) of *ca.* unity. The data were processed in the conventional manner using the Daresbury suite of EXAFS programs; EXCALIB, EXBACK[14] and EXCURV92.[15] Phase shifts were derived from *ab initio* calculations using the von Barth/Hedin-Lundqvist scheme within EXCURV92. The Fourier transforms were phase-corrected using the first shell (O) phase shift, therefore precise radial distances to other shells cannot be taken from the transform plots. The useful ***k***-space data is restricted to $k \approx 10$ Å^{-1} for the La L_{III} edge owing to the onset of the La_{II} edge. The data were Fourier filtered to include the range 1.5–5 Å of the Fourier transform which contains the dominant peaks. For each back-transformed spectrum a theoretical fit was obtained by adding shells of atoms around the central excited atom and iterating the radial distances, d, and the Debye–Waller (DW) type factors, $2\sigma^2$ (see Tables, later). This latter factor will contain contributions from both thermal disorder and static variations in d.

Results and Discussion

The previous ^{17}O solid-state NMR work in conjunction with powder XRD has shown that calcination of lanthanum carbonate yields La_2O_3 and that subsequent rehydration initially produces $La(OH)_3$ and then successive dehydroxylation gives LaO(OH) and then La_2O_3.[7] The starting point for the EXAFS work was examination of the model compounds La_2O_3, $La(OH)_3$ and LaO(OH) which had been characterised accurately by XRD analysis.

The EXAFS spectrum and its Fourier transform for a pure sample of La_2O_3 are shown in Fig. 1(*a*). This was a high-purity sample (Johnson-Matthey Ltd., 99.99%) that was dried under vacuum at 1000 °C and kept in a dry argon atmosphere. In the normal atmosphere La_2O_3 will absorb CO_2 and this will affect the EXAFS spectrum.[8] The crystallographic data for La_2O_3 are listed in Table 1.[16] There are too many shells to include in the EXAFS analysis given the limited ***k***-range of the data and hence a simplified three-shell model was chosen as the starting point of the EXAFS analysis, which has two oxygen shells at 2.39 and 2.73 Å and a single lanthanum shell at 3.89 Å. These parameters are based on weighted averages and are also shown in Table 1. The best-fit parameters to the EXAFS are shown as a dashed line in Fig. 1(*a*) and are also given in Table 1. The first EXAFS peak shows some definite structure indicating two distinct groupings of La–O distances and then a prominent La next-nearest-neighbour shell. The d values are close to the starting values, given an expected error in the fits of *ca.* ± 0.02 Å. The values of $2\sigma^2$ are reasonable given that they will include static variations in d for shells which are weighted averages of crystallographic values. The goodness of fit,[15] R, is also given in the Tables.

The EXAFS spectrum was collected for a sample of La_2O_3 produced by calcining lanthanum carbonate at 900 °C, as this should be more representative of the oxide produced by the gel route. This is shown in Fig. 1(*b*), the best fits are again shown as dashed lines and the fitted parameters are summarised in Table 1. There is some reduction in the intensity of the peaks in the Fourier transform which leads to somewhat higher DW factors in comparison with very pure La_2O_3. It should be emphasised that, given the high Debye temperature of such oxides relative to room temperature, the DW factors are probably dominated by static disorder. Again three shells are used and the structure of the La–O correlations into two shells is apparent. Hence these results provide some confidence in the overall EXAFS pattern expected from well defined La_2O_3.

Table 1 Structural parameters for the model compounds and best-fit EXAFS parameters

compound	diffraction data	simplified starting EXAFS model	best-fit EXAFS parameters			
			atom number and type	d/Å	$2\sigma^2$/Å^2	R (%)
La_2O_3	3[O] 2.365; 1[O] 2.456; 1[O] 2.731; 2[O] 2.732; 1[O] 3.680; 3[La] 3.786; 3[La] 3.851; 6[La] 3.938	4[O] 2.388; 3[O] 2.731; 12[La] 3.878	4 [O] 3 [O] 12 [La]	2.338 (2.328)[a] 2.705 (2.707) 3.881 (3.864)	0.016 (0.023) 0.002 (0.012) 0.019 (0.024)	21.0 (25.9)
$La(OH)_3$	1[O] 2.550; 2[O] 2.551; 4[O] 2.588; 2[O] 2.589; 2[La] 3.854; 2[O] 4.031; 1[O] 4.032; 2[La] 4.242; 4[La] 4.243	9[O] 2.577; 2[La] 3.854; 3[O] 4.032; 6[La] 4.243	9 [O] 3 [La] 3 [O] 6 [La]	2.568 3.892 3.896 4.316	0.022 0.008 0.031 0.022	26.8
LaOOH	1[O] 2.352; 1[O] 2.364; 2[O] 2.446; 1[O] 2.518; 2[O] 2.632; 4[La] 3.735; 2[La] 3.929; 1[O] 3.975; 1[O] 4.065; 2[La] 4.279	2[O] 2.358; 2[O] 2.446; 3[O] 2.594; 4[La] 3.735; 2[La] 3.929; 2[O] 4.020; 2[La] 4.279	4 [O] 3 [O] 4 [La] 2 [La] 2 [O] 2 [La]	2.508 2.675 3.829 3.907 4.283 4.317	0.003 0.004 0.024 0.007 0.016 0.010	22.1

[a]The numbers in brackets are the parameters for the sample of La_2O_3 prepared by calcining lanthanum carbonate at 900 °C.

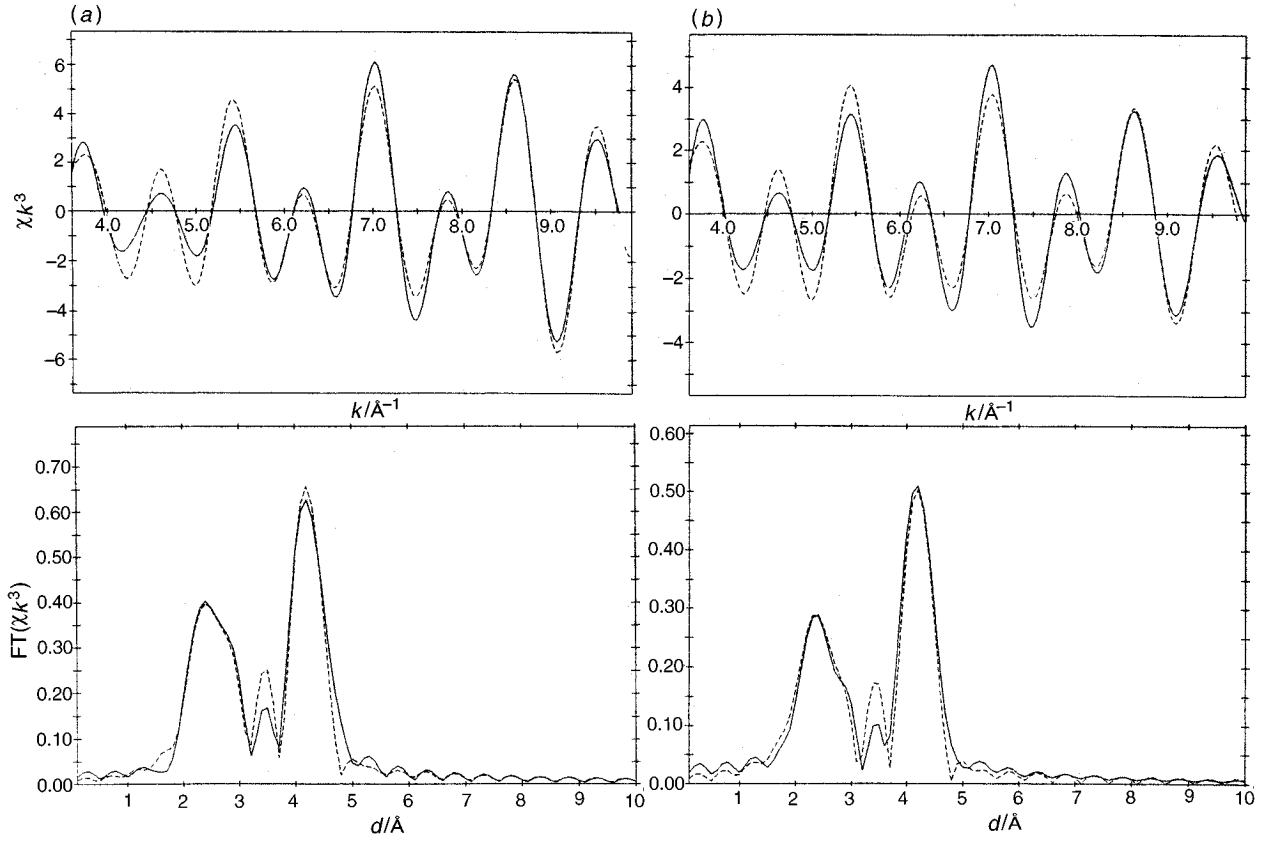

Fig. 1 La L_{III} edge EXAFS spectra (upper) and the corresponding Fourier transforms (lower) corrected with the phase shift of the first shell, showing the experimental data (solid line) and the best fit (dashed line) for (*a*) Johnson Matthey La_2O_3 and (*b*) La_2O_3 formed by calcination at 900 °C of $La_2(CO_3)_3$

The procedure described above was used to analyse the EXAFS spectra of $La(OH)_3$ and LaO(OH), shown in Fig. 2(*a*) and (*b*) respectively. It can be seen that the raw spectra from these two materials are very similar, reflecting the similarities of the La^{3+} environments in the two compounds which are characterised by a diffuse shell of several O^{2-} ions centred around 2.5–2.6 Å and a shell of several La^{3+} ions centred around 4 Å. Starting with distances taken from the crystal structures,[17–19] the best-fit parameters were found and these are listed in Table 1.

The EXAFS spectrum for an unheated gel collected at room temperature is shown in Fig. 3(*a*). Comparison of this spectrum with those from the model compounds indicates some similarities to La_2O_3, $La(OH)_3$ and LaO(OH). There are three peaks in the Fourier transform which with increasing *d* are presumably due to O^{2-}, O^{2-} and La^{3+}. The third peak is of significantly lower intensity for the gel than for any of the model compounds. Several strategies were explored to model the spectrum including (i) fixing the occupation numbers to be the same as in the three model compounds and floating *d* and σ^2, and (ii) also floating the coordination numbers. Not surprisingly, the latter approach gave the best fit. This model was improved further, although only slightly, by adding a fourth shell of La^{3+} ions. A reason for adopting this as the final model was evidence of a fourth shell in the heated gel samples (see later). The coordination numbers obtained from this fit were fixed at the closest integer values and the fitting repeated (*i.e.* floating *d* and σ^2) to yield the final set of parameters listed in Table 2. These indicate that although the gel is amorphous there is a very well ordered shell of O^{2-} ions at 2.53 Å, a distance similar to that of the first shell in $La(OH)_3$, around which there are much less ordered shells of O^{2-} and La^{3+} ions. However, the occupation of the first shell is only four, whereas it is nine for La^{3+} ions in aqueous solution and in $La(OH)_3$, reflecting the loose packing of the gel.

Heating the gel for periods of 1 h at successive temperatures of 100 and 200 °C caused no change in the EXAFS spectrum. However, in agreement with the NMR measurements, changes start to occur at 350 °C. The room-temperature EXAFS spectrum for the sample heated for 1 h at 350 °C is shown in Fig. 3(*b*). The striking feature is the reduced intensities of all the peaks in the Fourier transform when compared to the previous spectra. The simplest explanation is that at 350 °C the gel structure is transforming as the matrix collapses. The Fourier transform shows two main peaks at *ca.* 2.4 and 3.2 Å, and two small peaks at *ca.* 3.9 and 4.3 Å. These were fitted assuming the same coordination numbers as in the unheated gel and the final parameters are given in Table 2. The low intensity of the peaks for the outer shell may be due either to the highly disordered nature of the La^{3+} local environment or to the very small sizes of the crystallites of the intermediate that is being formed. However, the latter explanation would not be expected to hold for the first O^{2-} peak, as EXAFS studies of nanocrystalline oxides[20] usually exhibit a fully occupied and ordered first O^{2-} shell. Therefore it is suggested that the transformation at 350 °C involves a gross disruption of the structure to the extent that even the O^{2-} ions that are nearest neighbours of the La^{3+} ions are becoming disordered. As the ^{17}O NMR data indicate the formation of LaO(OH) at around 350 °C, it is interesting to compare the corresponding EXAFS results. The main similarity in the EXAFS is the radial distance to the first shell for the 350 °C sample and LaO(OH), as seen in Tables 1 and 2, although it would be optimistic to claim that the EXAFS evidence alone indicated that the latter compound was being formed as an intermediate.

Subsequent heating of the gel for 1 h at 700 °C showed

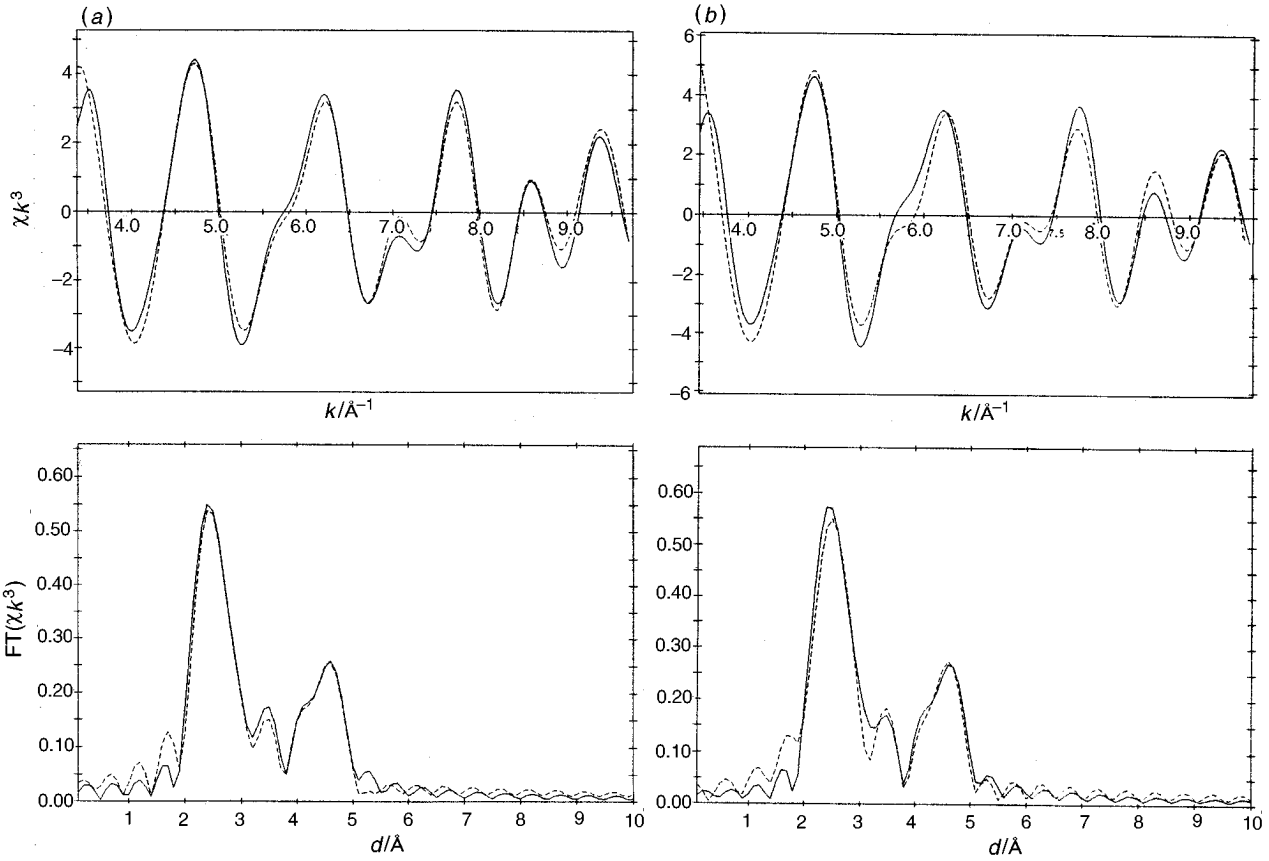

Fig. 2 La L_{III} edge EXAFS spectra (upper) and the corresponding Fourier transforms (lower) corrected with the phase shift of the first shell, showing the experimental data (solid line) and the best fit (dashed line) of (*a*) LaO(OH) and (*b*) $La(OH)_3$

Table 2 Simplified structural models and best-fit EXAFS parameters for La_2O_3 gels

	best-fit EXAFS parameters			
sample	atom number and type	*d*/Å	$2\sigma^2$/Å^2	*R* (%)
unheated gel at room temp.	4 [O]	2.534	0.011	19.5
	3 [O]	3.216	0.031	
	2 [La]	3.626	0.032	
	5 [La]	4.193	0.035	
gel heated for 1 h at 350 °C	4 [O]	2.493	0.036	33.1
	3 [O]	3.191	0.032	
	2 [La]	3.627	0.025	
	5 [La]	4.075	0.070	
gel heated for 1 h at 700 °C	4 [O]	2.414	0.028	22.7
	3 [O]	2.781	0.017	
	2 [La]	4.115	0.033	
	5 [La]	3.897	0.069	
gel heated for 1 h at 1000 °C	4 [O]	2.412	0.029	35.3
	3 [O]	2.762	0.019	
	2 [La]	4.094	0.052	
	5 [La]	3.937	0.025	

apparently only minor changes in the EXAFS spectrum, as seen in Fig. 4(*a*). However, fitting to the four-shell model showed that the two oxygen shells have moved significantly closer to the La^{3+} ion. The intensities of the two peaks due to the La^{3+} peaks have decreased slightly and the fitted Debye–Waller factors show a corresponding increase (Table 2). The ^{17}O NMR measurements indicate that La_2O_3 is forming at 700 °C. The XRD pattern for this sample yielded peaks that could be indexed to La_2O_3, although the peaks were broad. Analysis of the peak width using the Scherrer equation indicated a particle size of *ca.* 25–30 nm. The particles are therefore relatively large and the reduction in the intensity of the first peak of the Fourier transform cannot be explained solely in terms of crystallite size. A more realistic explanation is that the material is still highly disordered, accounting for both the EXAFS and the broad XRD peaks.

The room-temperature EXAFS spectrum of the sample heated for 1 h at 1000 °C is shown in Fig. 4(*b*). The best-fit parameters obtained by fitting to the four-shell model are shown in Table 2. The spectrum is now indicative of that for La_2O_3. The intensity of the near-neighbour O^{2-} shells is still low compared to that in the EXAFS of the high-purity La_2O_3 sample, but of similar magnitude to that in the calcined lanthanum carbonate. Although the intensity of the peak due to shells of the La^{3+} neighbours has increased significantly with a subsequent reduction in one of the corresponding

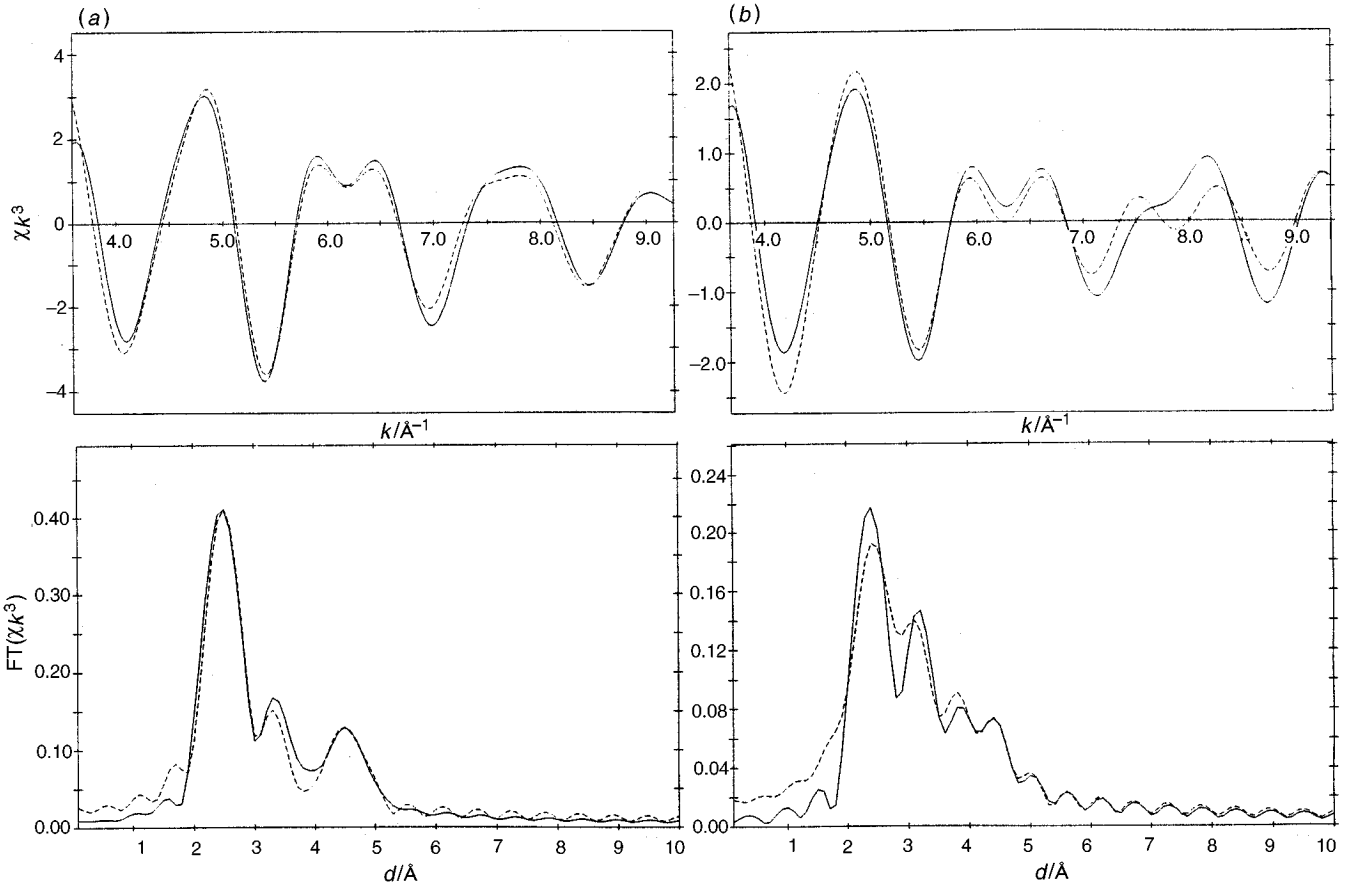

Fig. 3 La L_{III} edge EXAFS spectra (upper) and the corresponding Fourier transforms (lower) corrected with the phase shift of the first shell, showing the experimental data (solid line) and the best fit (dashed line) for La_2O_3 gel (*a*) unheated and (*b*) heated to 350 °C

Debye–Waller factors it is still smaller than that in the La_2O_3 samples. The XRD pattern of the sample indexed to La_2O_3, but the peaks were still broad. Analysis *via* the Scherrer equation indicated a particle size of *ca.* 70–100 nm; however, the broad peaks are more likely to be due to the disordered nature of the material.

The formation of La_2O_3 by thermal decomposition of the carbonate involves a structural breakdown through well defined intermediate stages, the EXAFS Debye–Waller factors indicating a high degree of order in the intermediates. At all stages along this route the next-nearest-neighbour (nnn) La–La correlations would seem to be maintained. The final product after calcining at 900 °C would appear to be slightly disordered on the EXAFS evidence. In contrast, the structural changes that occur in the gel would appear to involve highly disordered intermediates, with only very short-range order being retained between La^{3+} ions and the nearest-neighbour O^{2-} ions. Even the La_2O_3 formed from the gel at 700 °C shows only very weak La–La correlations and these are not truly representative of La_2O_3 in the gel sample heated at 1000 °C. A probable explanation is that the environment of the La^{3+} ions in the starting gel is very different to that in La_2O_3; the material is amorphous, there are fewer nearest-neighbour O^{2-} ions and they are at a longer distance. Heating the gel initially causes the structure to collapse and disrupt to the extent that there is even disorder in the first-shell O^{2-} ions around the La^{3-} ions. On further heating the 'fragments' will crystallise to form La_2O_3, a process involving lattice diffusion of the ions. The melting point of La_2O_3 is *ca.* 2300 °C, so the process will be very slow at 1000 °C, and it is not surprising that there is evidence of disorder in the gel heated at 1000 °C for 1 h.

It is interesting to compare the present EXAFS observations with the previous ^{17}O solid-state NMR work on gel-formed La_2O_3 samples. These two structural probes are using the alternative nuclei in the structure and both can be regarded as short-range structural probes. At 450 °C, although NMR shows that there is still some organic content, the gel has become largely LaO(OH) but the EXAFS pattern is not really characteristic of this phase [compare Fig. 2(*b*) and 3(*b*)] since although the oxygen shell is reasonably well defined the lanthanum shell is still smeared out. After heating to 700–800 °C the difference between the NMR and EXAFS data is even more striking. ^{17}O NMR shows that the oxygen environments have become like crystalline La_2O_3. The EXAFS would definitely agree with this for the O shells, but the La nnn shell is apparently very diffuse, as found in disordered materials. The implication is that in NMR the isotropic chemical shifts of the oxygen sites in a nanocrystalline sample produced from the gel have identical values and intensities as those from bulk La_2O_3. Hence, from ^{17}O NMR it is indicated that there is very little variation in the nearest-neighbour structure throughout the sample. The disorder must be largely in the nnn distance and beyond, which has very little influence on the ^{17}O NMR spectra. For the EXAFS the La–O shell is reasonably well defined, so again around the cation the very local structure is in place but there is still a large amount of static disorder that removes the La–La correlation. Hence the implication is that ^{17}O NMR shows that the local bonding is already La_2O_3-like and the disorder that occurs is in the linking of these units. It is worth noting that O EXAFS spectroscopy of materials has been reported recently.[21] It would be interesting to use this technique on the materials studied here, although such an experiment is not straightforward on such a light element. In particular, the comparison with ^{17}O NMR would be informative as the O EXAFS would be probing the local environment of the oxygen atoms and more could be said about the length-scale sensitivity of these two approaches. As is becoming increasingly clear, materials

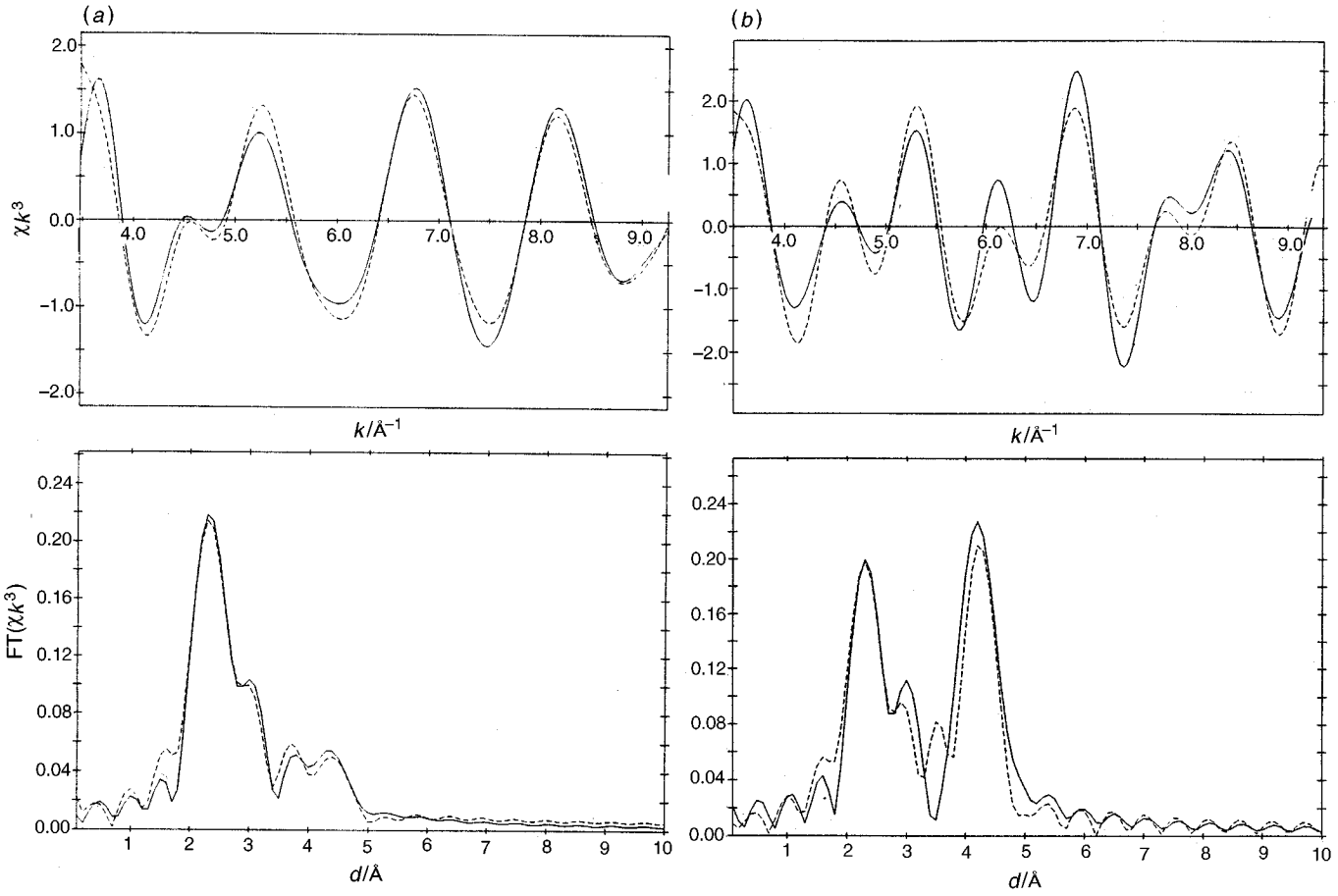

Fig. 4 La L_{III} edge EXAFS spectra (upper) and the corresponding Fourier transforms (lower) corrected with the phase shift of the first shell, showing the experimental data (solid line) and the best fit (dashed line) for La_2O_3 gel heated to (*a*) 700 °C and (*b*) 1000 °C

characterisation is improved greatly by using a combination of techniques. This paper represents one of the first comparisons of NMR and EXAFS approaches to structural studies of a gel-formed oxide.

Conclusions

This EXAFS study of the sol–gel route to La_2O_3 shows that on heating the gel, significant changes in structure begin to occur at around 350 °C. It was not possible to identify any specific intermediates from the EXAFS spectra alone, or the La_2O_3 that was produced at 700 °C. The reason for this was that the crystallites of La_2O_3 formed, and those of any intermediates, are highly statically disordered. This indicates that the eventual formation of La_2O_3 involves lattice diffusion, which is slow even at 1000 °C and explains the evidence for residual disorder in the La_2O_3 formed at this temperature.

This study highlighted some specific features of EXAFS and NMR as structural probes. The ^{17}O NMR of the same sol–gel process was able to identify clearly the nature of the intermediate phases, *e.g.* LaO(OH). Identification of the material by NMR relies on the chemical shift and hence the electron density caused by the local bonding. Thus, comparison of the NMR spectrum with those from model compounds is a fruitful procedure. In order to identify a material by EXAFS spectroscopy of the cation, one coordination shell is usually not sufficient, as can be seen from the similarity of the EXAFS spectra of LaO(OH) and $La(OH)_3$. For an unknown compound which is statically disordered, there will be reduced intensity of the peaks in the Fourier transform and therefore the spectrum will not match that for a well ordered model compound, making a direct comparison difficult.

The authors thank the EPSRC and CCLRC for provision of the beam time. F.A. thanks KISR (Kuwait) for providing a scholarship to study at Kent. Dr. G. Sankar (Royal Institution, London) is thanked for the loan of a furnace used in this work.

References

1 R. Birringer, H. Hahn, H. Hoefler, J. Karch and H. Gleiter, *Defect and Diffusion Forum*, 1988, **59**, 17.
2 D. C. Koningsberger and R. Prins, *X-Ray Absorption*, Wiley, London, 1988.
3 S. J. Gurman, in *Applications of Synchrotron Radiation*, ed. C. R. A. Catlow and G. N. Greaves, Blackie, London, 1993, p. 140; A. V. Chadwick, in *Applications of Synchrotron Radiation*, ed. C. R. A. Catlow and G. N. Greaves, Blackie, London, 1993, p. 171.
4 K. D. Campbell, H. Zhang and J. H. Lunsford, *J. Phys. Chem.*, 1988, **92**, 750.
5 Z. Kalinek and E. E. Wolf, *Catal. Lett.*, 1991, **9**, 441.
6 S. J. Milne, R. J. Brook and Y. S. Zhen, *Br. Ceram. Proc.*, 1989, **41**, 243.
7 F. Ali, M. E. Smith, S. Steuernagel and H. J. Whitfield, *J. Mater. Chem.*, 1996, **6**, 261.
8 P. Malet, M. J. Captian, M. A. Centano, J. A. Odriozola and I. Carrizoa, *J. Chem. Soc., Faraday Trans.*, 1994, **90**, 2783.
9 A. V. Chadwick, G. Morrison and R. Rafiuddin, *Radiat. Effects Defects Solids*, 1995, **134**, 91.
10 R. M. Almeida, M. I. Marques and M. C. Goncalves, *J. Non-Cryst. Solids*, 1994, **168**, 144.
11 E. M. Larson, A. J. G. Ellison, F. W. Lytle, A. Navrotsky, R. B. Greegor and J. Wong, *J. Non-Cryst. Solids*, 1990, **130**, 260.
12 S. Benazeth, M. H. Tuiler, A. M. Loireau-Lozac, H. Dexpert, P. Lagarde and J. Flattaut, *J. Non-Cryst. Solids*, 1989, **110**, 89.
13 F. J. Berry, S. Greaves, and R. C. Lobo, *J. Chem. Soc., Faraday Trans.*, 1991, **87**, 1405.

14 SERC Daresbury Program Library, 1991.
15 N. Binsted, J. W. Campbell, S. J. Gurman and P. C. Stephenson, SERC Daresbury Program Library, 1992.
16 D. J. Illet and M. S. Islam, *J. Chem. Soc*., *Faraday Trans*., 1993, **89**, 3833.
17 W. H. Zaichariasen, *Acta Crystallogr*., 1948, **1**, 265.
18 G. W. Beall, W. O. Milligan and H. A. Wolcott, *J. Inorg. Nucl. Chem*., 1977, **39**, 65.
19 P. V. Klevsov and L. P. Sheina, *Akad. Nauk SSSR Neorg. Mater*., 1965, **1**, 2219.
20 R. Nitsche, M. Winterer, M. Croft and H. Hahn, *Nucl. Instrum. Methods Phys. Res. Sect. B*, 1995, **97**, 127.
21 G. J. Baker, G. N. Greaves, M. Surman and M. Oversluizen, *Nuclear Instrum. Methods Phys. Res*., *Sect. B*, 1995, **97**, 375.

Paper 6/03547G; *Received* 21*st May*, 1996